The Journal of Engineering

IET International Radar Conference (IRC 2018)

IET Journals
The Institution of Engineering and Technology

Space scanning FMCW-based two-dimensional frequency diverse array radar

eISSN 2051-3305
Received on 20th February 2019
Accepted on 3rd May 2019
E-First on 15th August 2019
doi: 10.1049/joe.2019.0388
www.ietdl.org

Savaş Karadağ[1,2], Şimşek Demir[1,2] ✉, Altunkan Hızal[3]

[1]*Middle East Technical University, EEED, Ankara, Turkey*
[2]*PRF-R&D Inc., Technopark, METU, Ankara, Turkey*
[3]*Radar and Electronic Warfare Systems, Aselsan Inc., Ankara, Turkey*
✉ *E-mail: simsek@metu.edu.tr*

Abstract: The frequency-modulated continuous wave (FMCW)-based frequency diverse array (FDA) radar concept is extended to two dimensions (2D). The radar operates as a linear pulsed FMCW/FDA in the transmission (TX) mode while it operates as a pulsed FMCW/phased array (PA) in the receiving mode. It is shown that the FDA has the capability of scanning a 2D angular sector in a single pulse TX. It is shown that local instantaneous frequency bandwidth is much smaller than the radiofrequency (RF) frequency deviation of linear frequency modulation. Positive and negative slope TX/RF locations offer frequency diversity. The low signal-to-noise ratio of FDA is well compensated due to target temporal decorrelation diversity in the observation time and by the cumulative detection scheme used. Time domain and frequency domain signal processings are described. A Ku-band direct digital synthesis-based FDA radar design is compared by a corresponding equivalent PA radar.

1 Introduction

The frequency diverse array (FDA) concept [1, 2] was extended to a frequency-modulated continuous wave (FMCW)-based FDA in [3]. The FDA effect was obtained by applying a linear frequency modulation (LFM) chirp signal to the elements of a linear uniform array by progressive physical time delays T_{ℓ}, which was restricted to small values < 1 ns to reduce the size of the transmission (TX) lines. For space scanning, a two-dimensional (2D) linear FDA [4] was considered where the antenna beam scans, in particular, space trajectories. Here, we propose to use a hybrid direct digital synthesis (DDS) FMCW-based FDA to scan a 2D angular space. In Fig. 1, $T_{\ell x}$ and $T_{\ell z}$ are the progressive delays of the LFM applied to the antenna elements along x- and z-directions, respectively. The chirp length is τ and the radiofrequency (RF) frequency band width (FBW) is Δf. The chirp slope is $\mu_{\rm f} = \pm \Delta f/\tau$. For $T_{\ell z} \gg T_{\ell x}$, a 2D angular space scanning property of the FDA beam occurs. The FDA concept is used in TX only. In receiving (RX) digital beam forming (DBF) with phased array (PA) is proposed. A multiple pulsed FMCW/FDA radar in Ku-band is designed to illustrate the basic concepts such as fast scanning of 2D angular space in slow time. A cumulative radar detection scheme is proposed to overcome the low signal-to-noise ratio (SNR) of the FDA. The SNR for FDA per angle per pulse is smaller than that for PA by the energy ratio defined by $r_{\rm E} = E_{\rm o}^{\rm PA}/E_{\rm o}^{\rm FDA} \cong N \cdot \mathscr{K}_z$, where $\mathscr{K}_z = \Delta f T_{\ell z}$. We have also $\mathscr{K}_z \gg \mathscr{K}_x = \Delta f T_{\ell x}$. Moreover, the temporal decorrelation of the target in the long observation time provides a diversity gain. The local positions of the TX/RF for ± slopes for an angle are different, which gives an additional frequency diversity (FD).

Moreover, the bandwidths associated with a particular angle is much smaller than Δf. It is shown that for the example given, the FDA radar has less 2D angular scanning time and total energy-time product than that of the corresponding PA radar.

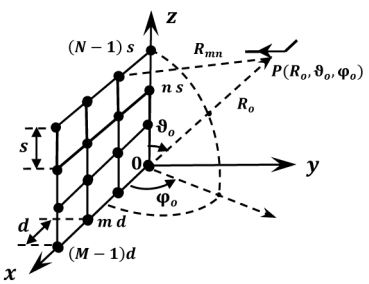

Fig. 1 *Linear 2D array with far field point*

2 Theory

A linear 2D array with M and N equidistant elements along x and z directions, respectively, is shown in Fig. 1. Each row in the x-direction is fed by DDS oscillators with delays $T_{\ell z}$. Along the x-direction, the elements are connected by corporate fed TX lines with delays $m\,T_{\ell x}$. The retarded time TX voltage at $P(R_{\rm o}, \vartheta_{\rm o}, \varphi_{\rm o})$ due to an antenna element at $\{x, z\}_{mn} = \{m \cdot d, n \cdot s\}$ can be expressed by

$$V_{mn}(t) = a_{mn}\exp\left[{\rm j}\left(\omega_o t'_{mn} + \frac{\mu}{2}t'^2_{mn}\right)\right] \cdot P(t'_{mn}, \tau) \tag{1}$$

where $\mu = 2\pi\mu_{\rm f}$. $\omega_{\rm o} = 2\pi f_{\rm o}$ is the carrier frequency, a_{mn} is the element weight. The frequency in (1) is $\omega(t) = \omega_{\rm o} + \mu t$ for the $\mu > 0$ (+ slope) and $\omega(t) = \omega_{\rm o} + \mu t + 2\pi\Delta f$ for the $\mu < 0$ (- slope). $t'_{mn} = t - R_{mn}/c - mT_{\ell x} - nT_{\ell z}$. c is the velocity of light. $P(t, \tau) = 1$ for $0 \le t \le \tau$ and 0 elsewhere. At $P(R_{\rm o}, \vartheta_{\rm o}, \varphi_{\rm o})$, $R_{mn} \cong R_{\rm o} - m\,d\sin\vartheta_{\rm o}\cos\varphi_{\rm o} - ns\cos\vartheta_{\rm o}$. Thus, the TX field can be shown to be

$$E_{\rm TX}(t') \cong A(t')\sum_{m=0}^{M-1} a_m\,{\rm e}^{{\rm j}m\gamma_x(t')}\sum_{n=0}^{N-1} b_n\,{\rm e}^{{\rm j}n\gamma_z(t')} \tag{2}$$

where

$$A(t') = \frac{f_{\rm e}(\vartheta_{\rm o}, \varphi_{\rm o})}{R_{\rm o}}P(t', \tau)\,{\rm e}^{{\rm j}\left(\omega_o t' + (\mu/2)t'^2\right)}, \quad f_{\rm e}(\vartheta_{\rm o}, \varphi_{\rm o})$$

is the wide band element pattern. $t' = t - R_{\rm o}/c$ is the retarded time. The + slope phase factors can be expressed by

$$\gamma_x^+(t') = -2\pi\nu_{ox}\left(\frac{t'}{T_f}+1\right);\quad \gamma_z^+(t') = -2\pi\nu_{oz}\left(\frac{t'}{T_f}+1\right) \tag{3}$$

$$\nu_{ox} = f_o T_{\ell x} - \frac{d}{\lambda_o}\sin\vartheta_o\cos\varphi_o;\quad \nu_{oz} = f_o T_{\ell z} - \frac{s}{\lambda_o}\cos\vartheta_o \tag{4}$$

λ_o is the wavelength. $T_f = f_o/\mu_f$. For the - slope, we add $\eta = \Delta f/f_o$ (relative RF FBW) into the parentheses in (3). For $a_m = b_n = 1$, the summations in (2) become

$$F_M = e^{j(M-1)\gamma_x/2}\sin(M\gamma_x/2)/\sin(\gamma_x/2) \tag{5}$$

$$F_N = e^{j(N-1)\gamma_z/2}\sin(N\gamma_z/2)/\sin(\gamma_z/2) \tag{6}$$

As the chirp signals arrive at elements at $t = mT_{\ell x} + nT_{\ell z}$ the array is filled up at $T_{fill} = (N-1)T_{\ell z}$. The LFM chirps applied to antenna elements are shown in Fig. 2. The fill time of the array should satisfy $T_{fill} \ll \tau$.

The build-up time (BUT) of the peak TX signal is obtained from (5) and (6) by setting $\gamma_{x,z}(t_o) = 2\pi\{p,q\}; p,q \in \mathbb{Z}$

$$t_{ox}^+ = T_f\cdot\left(\frac{-p}{\nu_{ox}}-1\right) > 0;\quad t_{oz}^+ = T_f\cdot\left(\frac{-q}{\nu_{oz}}-1\right) > 0 \tag{7}$$

For $\mu < 0$, we add $-\eta$ into the parentheses in (7). We should have $0 \le t_o' \le \tau$, which leads to $q_{min} \le q \le q_{max}$, and $q_{min} = -\mathrm{CE}\{(1+\eta)\nu_{oz}\}q_{max} = -\mathrm{CE}\{\nu_{oz}\}$, where CE stands for the ceiling integer. For a particular ϑ_o there is a finite set of values q. The BUT's of F_M and F_N must coincide. Equating $t_{ox}^{\pm} = t_{oz}^{\pm}$ yields

$$\cos\varphi_o = \left(f_o T_{\ell x} - \frac{p}{q}\cdot\nu_{oz}\right)/\left(\frac{d}{\lambda_o}\sin\vartheta_o\right) \tag{8}$$

This equation is solved for each value of q in the set for $-\mathrm{CE}\{(1+\eta)\times(f_o T_{\ell x} + s/\lambda_o)\} \le p \le -\mathrm{CE}\{f_o T_{\ell x} - s/\lambda_o\}$ and constraining $\cos\varphi_o \le 1$. This procedure associates a φ_o value with each q. It is found that $p = -\mathrm{CE}\{f_o\, T_{\ell x}\}$.

3 Numerical example

The FDA parameters are chosen with regard to the best waveforms and maximum 2D coverage The parameters are $f_o = 15.15\,\mathrm{GHz}, d/\lambda_o = s/\lambda_o = 0.5, M = 8,\ N = 5,\ \tau = 1\,\mathrm{ms}$, $T_{\ell x} = 0.2436\,\mathrm{ns}, T_{\ell z} = 2.04\,\mathrm{ns}$ and $\Delta f = 2999.7\,\mathrm{MHz}$. Then, we have $\eta = 0.198$, $T_f = \pm 5.051\,\mathrm{ms}$, $T_{fill} = 8.2\,\mathrm{ns}$, $f_o T_{\ell x} = 3.6905$, and $f_o T_{\ell z} = 30.906$. For a chosen cone angle of $\boldsymbol{\vartheta_o = 85°}$, we have six values of q, i.e. $\boldsymbol{q} \in \{-36, -35, \ldots, -31\}$.

Then, the corresponding BUTs for $0 < t_{oz}^+ < \tau$ are found as $t_{oz}^+ \in \{0.84, 0.68, 0.51, 0.35, 0.19, 0.023\}\,\mathrm{ms}$.

For $\vartheta_o = 85°$, $p = -4$, $\varphi_o \in \{58.4, 70.8, 83.1, 95.8, 109.6, 125.8\}°$. We have chosen Taylor tapering weights a_m in M for SLL $= -20\,\mathrm{dB}$, $\tilde{n}_m = 3$ and $b_n = 1$. The azimuth antenna beam widths (BWs) are $\boldsymbol{\varphi}_{oBW} = \{14.5,\ 13.4, 13.1, 13.5.14.7, 17.8\}°$. The elevation BWs corresponding to the azimuth values in the $\boldsymbol{\varphi_o}$ set are $\boldsymbol{\vartheta}_{oBW} = \{17.4,\ 17.8, 18.3, 18.8, 19.4, 20.0\}°$. Thus, the total angular coverage is ϑ_o: $\sim 76° \to 95°$ vertical and φ_o: $\sim 58° \to 126°$ azimuth yielding six number of φ_o TX beam positions (N_b). If we increment the cone angle $\boldsymbol{\vartheta}_o$ as $\boldsymbol{\vartheta}_o \in \{48,\ 66,\ \mathbf{85}, 103, 118, 132\}°$, ϑ_{oBW} and φ_{oBW} BWs do not leave a gap with $< -3\,\mathrm{dB}$ taper. The corresponding φ_o N_b's is six for each ϑ_o. Thus, the total N_b's is 36. The general coverage is ϑ_o: $\sim 38° \to 143°$ and φ_o: $\sim 30° \to 134°$, which is shown in Fig. 3. The dots correspond to the angles at which the BUT is a multiple of $\mathrm{CE}(T_{nn}) \cong 67\,\mu s$, where T_{nn} is the null-to-null time BW (TBW). At these points, multiple targets can be distinguished unambiguously in time.

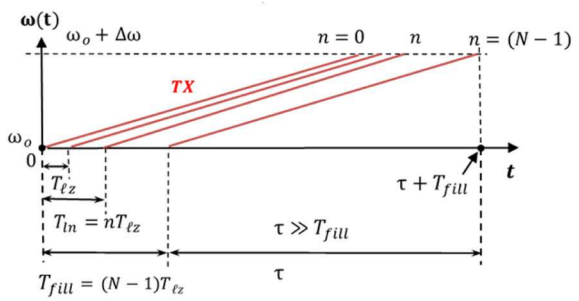

Fig. 2 *LFM chirps for antenna elements*

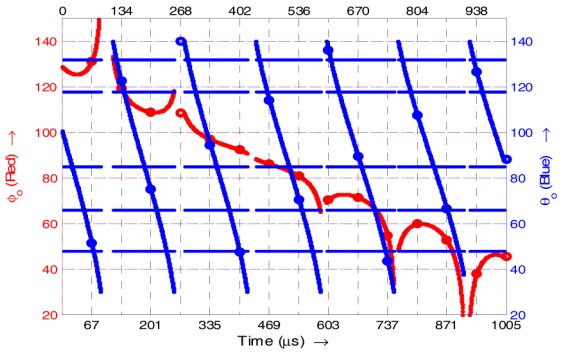

Fig. 3 *General coverage diagram*

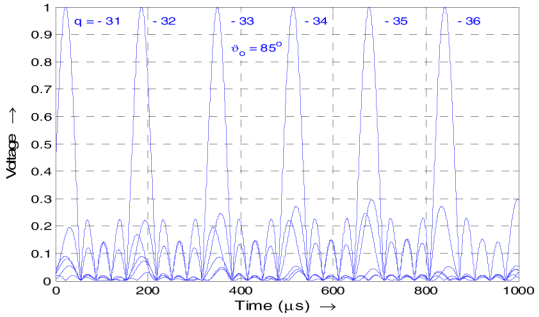

Fig. 4 *Normalised time-waveforms at $\vartheta_o = 85$*

The horizontal blue lines correspond to the cone angle $\boldsymbol{\vartheta}_o$ set. We can show that the null-to-null TBW T_{nnz} of F_N is expressed by $T_{nnz} = 2|T_f|/(N\,\nu_{oz}) \cong 2\tau/(\mathscr{K}_z N)$. For F_M, we have $T_{nnx} = 2|T_f|/(M\,\nu_{ox}) \cong 2\tau/(\mathscr{K}_x M)$, where the constants are $\mathscr{K}_z = 6.119$ and $\mathscr{K}_x = 0.731$. $\mathscr{K}_z$ approximately shows the number of φ_o antenna beams for each $\boldsymbol{\vartheta}_o$ and also the number of time waveforms in τ. For $\boldsymbol{\vartheta}_o = 85°$, we have $T_{nnz} = 66\,\mu s$ and $T_{nnx} \in \{368, 358, 348, 337, 327, 317\}\,\mu s$. In Fig. 3, we have $T_{nn} \cong T_{nnz} = 66\,\mu s$ and each BUT corresponds to a different value of φ_o. The time waveforms are shown in Fig. 4.

For the - slope, the results are the same except that the timings of the waveforms are reversed. The rate of rotation of the peak is found from (7) as

$$\Omega_{\vartheta_o} = \frac{\partial\vartheta_o}{\partial t} = \frac{\nu_{oz}^2}{qT_f(s/\lambda_o)\sin\vartheta_o} \cong \frac{\mathrm{sign}(\mu_f)\mathscr{K}_z}{\tau(s/\lambda_o)\sin\vartheta_o} \tag{9}$$

$$\Omega_{\varphi_o} = \frac{\partial\varphi_o}{\partial t} = \frac{\nu_{ox}^2}{pT_f(d/\lambda_o)\sin\vartheta_o\sin\varphi_o} \cong \frac{\mathrm{sign}(\mu_f)\mathscr{K}_x}{\tau(d/\lambda_o)\sin\vartheta_o\sin\varphi_o} \tag{10}$$

Since $\mathscr{K}_z \gg \mathscr{K}_x$, we have $\Omega_{\vartheta_o} \gg \Omega_{\varphi_o}$. A separate very similar RX PA antenna with sufficient isolation receives the echo signal from a target. The RX signal is obtained by mixing (dechirping) the received echo by a coherent local oscillator (LO) chirp with

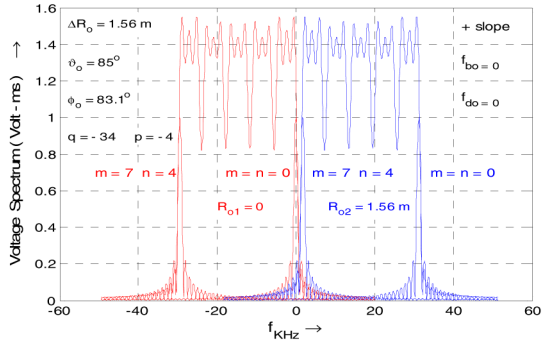

Fig. 5 *$\mathcal{FT}$ spectrum for + slope and $\vartheta_o = 80°; \varphi_o = 83.1°$*

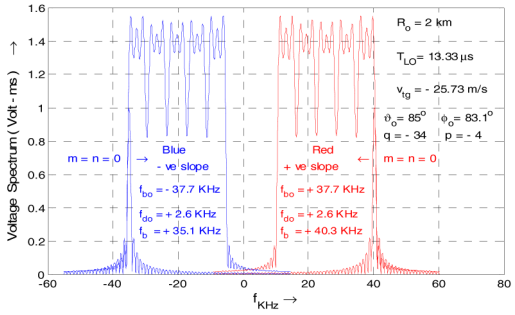

Fig. 6 *$\mathcal{FT}$ spectrum for ± slopes with range and Doppler*

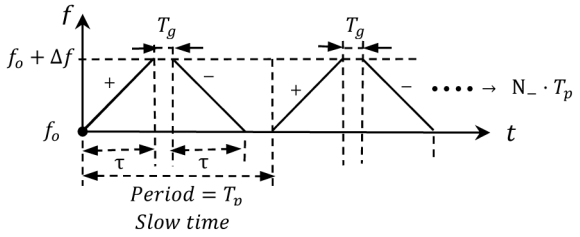

Fig. 7 *Periodic coherent ± slope N_- radar pulses*

duration $\tau_{\rm LO} \geq \tau + T_{\rm do} + T_{\rm fill} - T_{\rm LO}$, where $T_{\rm LO}$ is the time offset for the beat frequency (BF) $\omega_{\rm bo} = 2\pi\, f_{\rm bo} = \mu(T_{\rm do} - T_{\rm LO})$. The base band signal is the same as the classical FMCW signal with an FDA envelope

$$V^+(t') \cong \mathbb{V}_{\rm o}(t) \sum_{m=0}^{M-1} a_m \, {\rm e}^{{\rm j}m\gamma_x^+(t')} \sum_{n=0}^{N-1} b_n \, {\rm e}^{{\rm j}n\gamma_z^+(t')} \tag{11}$$

$\mathbb{V}_{\rm o}(t) = V_{\rm o}\, {\rm e}^{{\rm j}\psi(t')} P(t', \tau)$, $t' = t - T_{\rm do}$ and $\psi(t) \cong \omega_{\rm b} t$ with the effective BF $\omega_{\rm b} = \omega_{\rm bo} + \omega_{\rm do}$ and $\omega_{\rm do} = 2\pi f_{\rm do} = 2\omega_{\rm o} v_{\rm tg}/c$ is the Doppler frequency (DF) for an outgoing target with radial velocity $v_{\rm tg} > 0$. $V_{\rm o}$ is the complex amplitude containing the amplitude and phase of the radar RX/RX functions and the propagation path. The Fourier transform ($\mathcal{FT}$) of $V^+(t')$ is

$$\tilde{V}^+(\omega) = \tilde{\mathbb{V}}_{\rm o} \sum_{m=0}^{M-1} \sum_{n=0}^{M-1} a_m b_n \, {\rm e}^{-{\rm j}2\pi(\Psi_{mn} + (\bar{\omega}\tau/4\pi))} \frac{\sin(\bar{\omega}\tau/2)}{\bar{\omega}\tau/2} \tag{12}$$

$\tilde{\mathbb{V}}_{\rm o} = V_{\rm o}\tau\, {\rm e}^{-{\rm j}\omega T_{\rm do}}$, $\Psi_{mn} = m\nu_{ox} + n\nu_{oz}$, $\bar{\omega} = \omega - \omega_{\rm b} + \omega_{mnf}$ and $\omega_{mnf} = m\,\omega_{fx} + n\omega_{fz}$. The spectral components (SCs) are $\omega_{fx} = 2\pi\nu_{ox}/T_{\rm f} \ll \omega_{fz} = 2\pi\nu_{oz}/T_{\rm f}$. For the - slope, Ψ_{mn} is replaced by $(1+\eta)\Psi_{mn}$. The centre frequency of the (m,n)th SC is $\bar{\omega}_{mnc} = \pm\omega_{\rm bo} + \omega_{\rm do} - \omega_{mnf}$. The SCs are orthogonal if $\mathscr{K}_z$ and $\mathscr{K}_x$ are integers. In this case, the peak of a SC coincides with the nearest $\mathscr{K}_{z,x}^{\rm th}$ null of the adjacent one. Here $\mathscr{K}_z = 6.119$ and $\mathscr{K}_x = 0.731$. Thus, there is approximate spectral orthogonality. In the frequency domain ($\mathcal{FD}$), the FBW is given by

$$\omega_{\rm BW} = (M-1)\omega_{fx} + (N-1)\omega_{fz} + \frac{2\pi}{\tau} \cong \frac{(N-1)\mathscr{K}_z + 2}{\tau/(2\pi)} \tag{13}$$

$\omega_{\rm BW} = 2\pi f_{\rm BW}$. If two targets are separated by $\Delta R_{\rm o}$ such that their Fourier spectra ($\mathcal{FS}'$s) are adjacent to each other, then we should have the BF increment $\Delta f_{\rm bo} = f_{\rm BW}$, which leads to $\Delta R_o = \tau f_{\rm BW} c/(2\Delta f) \cong (N-1)cT_{\ell z}/2 + c/\Delta f$. In the present case, $f_{\rm BW} = 31.2\,{\rm kHz}$ and $\Delta R_{\rm o} = 1.573\,{\rm m}$. The time periods of the F_N and F_M waveforms at an angle $\vartheta_{\rm o}$ are $T_{pz} = T_{\rm f}/\nu_{oz} \cong \tau/\mathscr{K}_z < \tau$ and $T_{px} = T_{\rm f}/\nu_{ox} \cong \tau/\mathscr{K}_x > \tau$. For $\vartheta_{\rm o} = 85°$, $T_{pz} = 0.16\,{\rm ms}$ and $T_{px} = \{1.27 \rightarrow 1.47\}{\rm ms}$. Thus, only the first peaks of F_M coincide with the periodic $\sim \mathscr{K}_z$ peaks of F_N in τ. The difference of the BUTs for the ± slopes is $\Delta t_{\rm o} = t_{oz}^+ - t_{oz}^- = -|T_{\rm f}|(2q/\nu_{oz} + 2 + \eta)$, which can be solved for $\vartheta_{\rm o}$ using the conditions $q \cong -{\rm CE}(f_o T_{\ell z})$ and $\cos\vartheta_{\rm o} = f_o T_{\ell z} + q/[1 + 0.5(\Delta t_o/|T_{\rm f}| + \eta)] < 1$. $\varphi_{\rm o}$ is found from $\cos\varphi_{\rm o} = f_o T_{\ell x} + p/[1 + 0.5(\Delta t_o/|T_{\rm f}| + \eta)]$ using the conditions $p \cong -{\rm CE}(f_o T_{\ell x})$ and $\cos\varphi_{\rm o} < 1$. The sum of the time of arrivals for ± slopes is a function of range only. The sum $\Sigma t_{\rm o} = t_{oz}^+ + t_{oz}^- = 4R_{\rm o}/c + |T_{\rm f}|\eta$. The range resolution in the time domain ($\mathcal{TD}$) is not realistic since $\Delta R_{\rm o}(T_{\rm nn}) = cT_{\rm nn}/4 = 5\,{\rm km}$ is very large. Thus, the range should be found from the $\mathcal{FD}$ processing. For multiple targets, the angles should be determined by RX beams.

Two targets at points $R_{o1}, \vartheta_{o1}, \varphi_{o1}$ and $R_{o2}, \vartheta_{o2}, \varphi_{o2}$ may have the same time of arrivals, i.e. $T_{do1} + t_{oz1}^+ = T_{do2} + t_{oz2}^+$. The difference between the ranges is from $\Delta t_{oz1}^+ = t_{oz1}^+ - + t_{oz2}^+$, $\Delta R_{o21}^+ = R_{o2} - R_{o1} = (cT_{\rm f}/2)(q_1/\nu_{oz1} - q_2/\nu_{oz2})$. At $\vartheta_{\rm o}$, we have $\Delta R_{o21}^+ \cong [cT_{\rm f}/(f_o T_{\ell z})](s/\lambda_{\rm o})\sin\vartheta_{\rm o}\sin(\vartheta_{\rm oBW}/2)$, where the target angles are $\vartheta_{o1,2} = \vartheta_{\rm o} \mp \vartheta_{\rm oBW}/2$. Since $\Delta R_{o21}^+ \gg \Delta R_{\rm o}$, these targets cannot be distinguished in $\mathcal{TD}$ and the angle finding algorithm described above will not work. However, in $\mathcal{FD}$, they will be separated by $\Delta\omega_{b12}$, hence $\Delta R_{\rm o}$ will work. The $\mathcal{FT}$ of the FDA waveform for uniform weights for two targets separated by $\Delta R_{\rm o}$ is shown in Fig. 5. For the - slope, the edges related to $m = M-1$ and $n = N-1$ shift to the right of the edges for $m = n = 0$. The BF due to the range and +DF due to – velocity (closing in target) shifts the spectra as shown in Fig. 6. The BF is large as the slope $\mu_f = \pm 2.9997\,{\rm MHz}/\mu{\rm s}$ is very steep. For $R_{\rm o} = 2\,{\rm km}$, $T_{\rm do} = 13.34\,\mu{\rm s}$ and $f_{\rm bo} = 40.02\,{\rm MHz}$. For $T_{\rm LO} = 13.3\,\mu{\rm s}$, it is reduced to $f_{\rm bo} = 37.7\,{\rm kHz}$. The BFs are $f_{b\pm} = f_{\rm bo} \pm f_{\rm do}$. By measuring $f_{b\pm}$, we can obtain both $f_{\rm bo}$ and $f_{\rm do}$, which enables us to find both $R_{\rm o}$ and $v_{\rm tg}$. The measurement accuracy depends on ${\rm SNR} = E_{\rm o}/\eta_{\rm o}$, where $E_{\rm o}$ is the energy of the FDA waveform and $\eta_{\rm o} = kT_{\rm s}$ is the noise spectrum density, k is the Boltzmann's constant and $T_{\rm s}$ is the noise temperature in Kelvin. $E_{\rm o}$ is the area of the square of $\mathcal{FS}$ and for uniform weights $E_{\rm o} = 53.9\,{\rm mJ/V_o^2}$. Also, $E_{\rm o} \cong M^2 N V_{\rm o}^2 \tau/\mathscr{K}_z$. Finding the coherent average of $\mathcal{FT}$ recovers $E_{\rm o}$. This procedure is a matched filtering in $\mathcal{FT}$ domain. As the chirps are coherent for Swerling I (SW I) targets, Doppler filters (DFL) are formed by applying another $\mathcal{FT}_{\rm D}$ for N_- coherent ± pulses. This is the 2D $\mathcal{FT}$ used in FMCW radars [5]. N_- ± slope pulses are shown in Fig. 7. $T_{\rm g} > T_{\rm do}$ is required for dechirping and pulse sampling. The phase of the nth pulse is given by $\psi_n[t' + (n-1)T] = \omega_{bn}t' + \alpha_n + \Phi_{\rm d}$, where $0 \leq t' \leq \tau$, $\omega_{bn} = \omega_{\rm bo} + \omega_{\rm do} + \Delta\varpi_{bn}$, $\Delta\varpi_{bn} = \mu(n-1)v_{\rm tg}T$ $\alpha_n = -\Delta\varpi_{bn}[2R_{\rm o}/c + (n-1)v_{\rm tg}T/c]$ and $\Phi_{\rm d} = (n-1)\omega_{\rm do}$.

Then, in (11) and (12), $\psi \rightarrow \psi_n$ and $\tilde{V}^+(\bar{\omega}) \rightarrow V^+(\omega - \omega_{bn})$. $\tilde{V}^+(\omega - \omega_{bn})$ and $\mathcal{FT}_{\rm D}$ should be found by a discrete $\mathcal{FT}$; $\omega = \omega_i$; $i = 1, \ldots, i_{\max}$, which is the total number of samples

$$\check{V}_{\mathscr{K}i} = \sum_{n=0}^{N_- - 1} \tilde{V}(\omega_i - \omega_{bn})\, {\rm e}^{-{\rm j}2\pi(n-1)\,\mathscr{K}_i/N_- - {\rm j}\alpha_n} \tag{14}$$

forms for $\mathscr{k} = 0, 1, \ldots, N_- - 1$, N_- DFL's with period $2\pi/T$, the null-to-null BW $4\pi/(N_-T)$ and the centre frequency $\omega_{c\mathscr{k}} = 2\pi\mathscr{k}/(N_-T)$. The inclusion of α_n implies velocity compensated DFL. This requires a velocity estimation, which can be achieved either from the ± slope range $\mathcal{FT}$ or forming complex signal $V_{cn}(t') = V_n(t') + \mathrm{j}\hat{V}_n(t')$, where $\hat{V}_n(t')$ is the Hilbert transform of $V_n(t')$. If Φ_n is the phase of $V_{cn}(t')$, we can show that $\Delta\Phi_n = \psi_{n+1} - \psi_n \cong \omega_{\mathrm{do}}T$. We have found that α_n can be ignored in most cases for $N_- \lesssim 32$.

4 Radar example

The size of the TX/RX antenna is ~ 8 cm × 5 cm. The patterns for wide band microstrip patch elements are shown in Fig. 8. The antenna gain is $G_{\mathrm{A}} = 21.3$ dB. The parameters other than those given in Section 3, are $N_- = N_-^{\mathrm{FDA}} = 8$ coherent pair of ± pulses form a burst. There are $n_-^{\mathrm{FDA}} = 24$ non-coherent bursts. $T_{\mathrm{g}} = 250\,\mu$s and $T_{\mathrm{p}} = 2500\,\mu$s. The duty cycle is 80%. The radar range equation for noise only can be written as

$$\mathrm{SNR} = \frac{E_{\mathrm{ot}}}{r_{\mathrm{E}}\ k\ \mathrm{T_s}} \cdot \frac{G_{\mathrm{A}}^2\sigma_{\mathrm{s}}\lambda_{\mathrm{o}}^2 L_{\mathrm{t}}L_{\mathrm{a}}}{(4\pi)^3 R_{\mathrm{o}}^4} = \frac{D_{\mathrm{l}} \cdot L_x}{I_{N_-} \cdot G_i \cdot G_{\mathrm{div}}} \tag{15}$$

$E_{\mathrm{ot}} = 2P_{\mathrm{t}}\tau$; $2P_{\mathrm{t}} = 10$ W. $r_{\mathrm{E}} = 29.68$ is the energy ratio. $L_{\mathrm{t}} = 2$ dB is the TX loss, $L_{\mathrm{a}} = 0.096$ dB is the atmospheric loss. $R_{\mathrm{o}} = 2$ km. The noise energy is $kT_{\mathrm{s}} = 9.16 \times 10^{-18}$ mJ.

We consider a SW I target of radial extent $L_{\mathrm{tg}} = 1$ m and radial velocity $v_{\mathrm{tg}} = -25.72$ m/s with RCS $\sigma_{\mathrm{s}} = 0.1$ m^2 and decorrelation time $T_{\mathrm{ctg}} \cong 100$ ms [6]. In TX modules, $N = 5$ DDS oscillators will provide the delays $T_{\ell z}$ and outputs should be upconverted to f_{o}. The delays $T_{\ell x}$ will be provided by TX lines on a substrate with a high-dielectric constant. In the RX modules, LO down conversion to the base band and signal processing based on 2D $\mathcal{FT}$ should be combined with DBF. We need $N_{\mathrm{b}} = 36$ RX beams to cover the 2D angular space. The FDA TX beam scans this sector in T_{p}. In (15), $L_x = 3$ dB is the processing loss. I_{N_-} is the SNR improvement factor of cascaded single delay line canceller filter and DFL. v_{tg} and T_{p} are chosen for maximum $I_{N_-} = 8.533$. The DF is $f_{\mathrm{do}} = 2.6$ kHz. For $T_{\mathrm{LO}} = 13.276\,\mu$s, $f_{\mathrm{bo}} = 200$ kHz. The sampling frequency is $f_{\mathrm{s}} \geq 2f_{\mathrm{bo}}$. D_{l} is the detectability factor for a SW I target in noise expressed by $D_{\mathrm{l}} = \log_{\mathrm{e}}(P_{\mathrm{fa}})/\log_{\mathrm{e}}(P_{\mathrm{d}}) - 1$, where P_{d} is the probability of detection and P_{fa} is the probability of false alarm. The coherent integration time is $\mathrm{CTI}^{\mathrm{FDA}} = 22.26$ ms. Since $L_{\mathrm{tg}} \leq \Delta R_{\mathrm{o}} - |v_{\mathrm{tg}}|\mathrm{CTI}^{\mathrm{FDA}} \cong 1$ m, the target will remain within ΔR_{o} in $\mathrm{CTI}^{\mathrm{FDA}}$. The frame time (FRT) for n_-^{FDA} bursts is $\mathrm{FRT}^{\mathrm{FDA}} = n_-^{\mathrm{FDA}}\mathrm{CTI}^{\mathrm{FDA}} \cong 534.3$ ms in which the target decorrelates by $n_{\mathrm{ctg}} = \mathrm{FRT}^{\mathrm{FDA}}/T_{\mathrm{ctg}} = 5$ times. If we make a detection trial at the end of each $\mathrm{FRT}^{\mathrm{FDA}}$, i.e. in each cumulative detection step (CDS). In $n_{\mathrm{s}}^{\mathrm{FDA}}$ CDSs, we have

$$P_{\mathrm{cd}}^{\mathrm{FDA}} = 1 - (1 - P_{\mathrm{d}})^{n_{\mathrm{s}}^{\mathrm{FDA}}} \quad P_{\mathrm{cfa}}^{\mathrm{FDA}} = 1 - (1 - P_{\mathrm{fa}})^{n_{\mathrm{s}}^{\mathrm{FDA}}} \tag{16}$$

For the chosen radar parameters, the solution of (15) for $n_{\mathrm{s}}^{\mathrm{FDA}} = 2$ becomes $P_{\mathrm{d}} = 0.8346$ for $P_{\mathrm{fa}} = 0.5 \times 10^{-6}$. Thus from (16), we have $P_{\mathrm{cd}}^{\mathrm{FDA}} = 0.9727$ and $P_{\mathrm{cfa}}^{\mathrm{FDA}} = 10^{-6}$. $\mathrm{SNR}^{\mathrm{FDA}} = 16.8$ dB in the $\mathrm{FRT}^{\mathrm{FDA}}$. The non-coherent integration gain for n_-^{FDA} bursts for P_{d} and P_{fa} is $G_i^{\mathrm{FDA}} = 10.58$ dB. The diversity gain for $N_{\mathrm{div}}^{\mathrm{FDA}} = 5 \times 2 = 10$ becomes $G_{\mathrm{div}}^{\mathrm{FDA}} = 5.48$ dB which stems from n_{ctg} and also a two-fold ± slope FD.

The BUT's for ± slopes are different causing different $f_{\mathrm{oFDA}}^{\pm}$ centre frequency locations in the chirp. $|f_{\mathrm{oFDA}}^{+} - f_{\mathrm{oFDA}}^{-}| > f_{\mathrm{c}}$, where $f_{\mathrm{c}} \cong c/(2L_{\mathrm{tg}}) = 150$ MHz is the decorrelation frequency of a SW I target, yielding a two-fold FD. The local chirp FBW at $f_{\mathrm{oFDA}}^{\pm}$

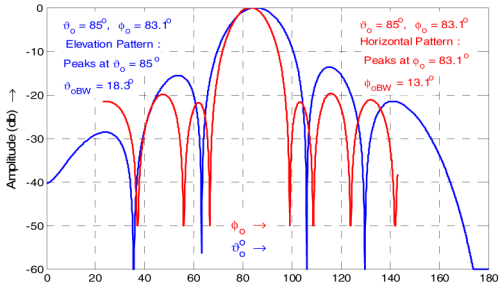

Fig. 8 *Antenna patterns*

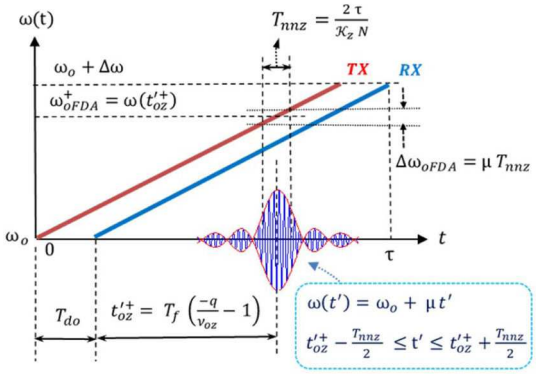

Fig. 9 *RF and bandwidth for a particular angle for + slope*

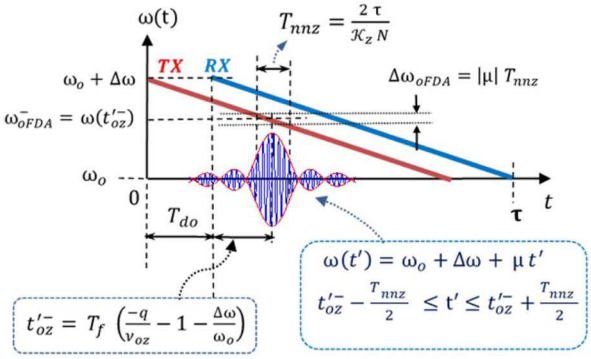

Fig. 10 *RF and bandwidth for a particular angle for − lope*

is $\Delta f_{\mathrm{oFDA}} \cong |\mu_{\mathrm{f}}|T_{\mathrm{nnz}}/2$, where $T_{\mathrm{nn}z}/2$ is the energy equivalent TBW.

The local behaviour of FBW for ± slopes are shown in Figs. 9 and 10. Since $\Delta f_{\mathrm{oFDA}} \cong 98.9\,\mathrm{MHz} < f_{\mathrm{c}}$, an intrapulse FD does not occur. The final detection is made in the waveform time $\mathrm{WFT}^{\mathrm{FDA}} = n_{\mathrm{s}}^{\mathrm{FDA}} \cdot \mathrm{FRT}^{\mathrm{FDA}} = T_{\mathrm{rv}}^{\mathrm{FDA}} = 1068$ ms.

5 Discussion

Let us compare the present FMCW/FDA radar with an equivalent FMCW/PA radar. The parameters for PA are $N_- = N_-^{\mathrm{PA}} = 8$, $n_-^{\mathrm{PA}} = 2$, $n_{\mathrm{s}}^{\mathrm{PA}} = 1$, and $\Delta f^{\mathrm{PA}} = 95.296$ MHz. $N_{\mathrm{div}}^{\mathrm{PA}} = 2$ frequency agility steps from burst-to-burst are used for PA, r_{E} in (15) is to be removed. The solution of (15) yields $P_{\mathrm{d}} = 0.9708$ for $P_{\mathrm{fa}} = 10^{-6}$. We have $G_i^{\mathrm{PA}} = 2.7$ dB and $G_{\mathrm{div}}^{\mathrm{PA}} = 6.35$ dB. For $N_-^{\mathrm{PA}} = 8$, we have $\mathrm{CIT}^{\mathrm{PA}} = 22.26$ ms and $\mathrm{FRT}^{\mathrm{PA}} = \mathrm{WFT}^{\mathrm{PA}} = 44.53$ ms. Since the required number of TX beam positions are $N_{\mathrm{b}} = 36$, the revisit time of a target is $T_{\mathrm{rv}}^{\mathrm{PA}} = N_{\mathrm{b}} \times \mathrm{WFT}^{\mathrm{PA}} = 1603$ ms with $\mathrm{SNR}^{\mathrm{PA}} = 23.65$ dB.

If we do not use a cumulative detection in FDA, we would have $T_{\mathrm{rv}}^{\mathrm{FDA}} = 534.3$ ms with $\mathrm{SNR}^{\mathrm{FDA}} = 16.8$ dB and the target would move 13.74 m and 41.35 m in $T_{\mathrm{rv}}^{\mathrm{FDA}}$ and $T_{\mathrm{rv}}^{\mathrm{PA}}$, respectively. This property may be an advantage in FDA radar for tracking a high radar cross-section target.

We will also compare the FDA and PA equivalent radars from the energy-time product point of view. The energy input to the two radars is the same $E_{\text{oin}} = E_{\text{ot}}$. The total power delivered to the radars in the revisit times are

$$E_{\text{oT}}^{\text{FDA}} = E_{\text{oin}} \quad N_{-}^{\text{FDA}} n_{-}^{\text{FDA}} n_{\text{s}}^{\text{FDA}} = 384 E_{\text{oin}} \tag{17}$$

$$E_{\text{oT}}^{\text{PA}} = E_{\text{oin}} \quad N_{-}^{\text{PA}} n_{-}^{\text{PA}} n_{\text{s}}^{\text{PA}} \quad N_{\text{b}} = 576 E_{\text{oin}} \tag{18}$$

$$E_{\text{oT}}^{\text{FDA}} / E_{\text{oT}}^{\text{PA}} = 2/3 = 0.666 \tag{19}$$

$$\left(E_{\text{oT}}^{\text{FDA}} \cdot T_{\text{rv}}^{\text{FDA}}\right) / \left(E_{\text{oT}}^{\text{PA}} \cdot T_{\text{rv}}^{\text{PA}}\right) = 4/9 = 0.444 \tag{20}$$

Thus, it is seen that the present FDA radar has less energy-time product compared to the equivalent PA radar. This conclusion, however, should not be generalised to all cases of FDA/PA comparisons.

6 Conclusions

The FDA radar distributes the energy to time and space has a low probability of intercept property. Also, different TX f_{oFDA} centre frequencies for each scanning angle may be interpreted as a frequency scan. The space scanning property can be exploited by a cumulative detection scheme to compensate for the reduced SNR inherent in all FDA-based radars. Also, the long observation time of the target provides a temporal diversity gain. Using the $\mathcal{FT}$ domain range Doppler signal processing, we can determine the range and Doppler of targets conveniently. The implementation of such a radar requires a hybrid feed topology, i.e. for $T_{\ell x}$ (low) TX lines, while for $T_{\ell z}$ (high) DDSs are required. The target's direction can be conveniently found by RX beams.

7 Acknowledgments

The authors thank the Middle East Technical University and Aselsan Inc. for the support given to this work.

8 References

[1] Antonik, P., Wicks, M.C., Griffiths, H.D., *et al.*: 'Frequency diverse array radars'. IEEE Radar Conf., Verona, NY, USA, 2006, pp. 215–217

[2] Secmen, M., Demir, S., Hizal, A., *et al.*: 'Frequency diverse array antenna with periodic time modulated pattern in range and angle'. IEEE Radar Conf., Boston, MA, USA, 2007, pp. 427–430

[3] Eker, A.T., Demir, S., Hizal, A.: 'Exploitation of linear frequency modulated continuous waveform LFMCW for frequency diverse arrays', *IEEE Trans. Antennas Propag.*, 2013, **61**, pp. 3546–3553

[4] Cetiner, R., Hizal, A.: 'Narrow band wide angle scanning two dimensional frequency diverse array radar'. IET Int. Radar Conf., Belfast, UK, 2017

[5] Khan, R.H., Power, D.: 'Doppler processing for coherent chirp radars'. Proc. Canadian Conf. on Electrical and Computer Engineering, Halifax, Canada, September 1994, vol. 2, pp. 767–770

[6] Edrington, T.S.: 'The amplitude statistics of aircraft radar echoes', *IEEE Trans. Mil. Electron.*, 1965, **9**, (1), pp. 10–16